Proceedings of the
Annual Stability Conference
Structural Stability Research Council
San Antonio, Texas, March 19-22, 2024

Buckling analysis of cold-formed steel built-up columns using Generalized Beam Theory

Cilmar Basaglia[1], Dinar Camotim[2], Rodrigo Gonçalves[3]

Abstract

This paper reports the available results of an ongoing investigation on the use of Generalized Beam Theory (GBT) to assess the buckling behavior of cold-formed steel built-up members connected by discrete fasteners. After an overview of the main concepts and procedures involved in performing GBT buckling analyses, the paper presents the formulation and implementation of a GBT-based beam finite element accounting for the presence of discrete fasteners by means of constraint equations (an approach that constitutes a first step towards more realistic fastener simulations) – particular attention is devoted to the determination of the stiffness and geometric matrices. In order to illustrate the application and evidence the potential and advantages of the proposed approach, namely concerning its ability to provide in-depth information on the mechanics of instability in built-up members, several illustrative examples are presented and discussed in detail – they deal with columns built-up from two or three lipped channel profiles. For the sake of validation, most of the GBT-based results obtained are compared with values yielded by rigorous ("exact") ANSYS shell finite element analyses – a virtually perfect match is invariably found.

1. Introduction

The extensive use of cold-formed steel (CFS) members in the construction industry stems mostly from their high structural efficiency (large strength-to-weight ratio), remarkable fabrication versatility and very low production and erection costs. In recent years, the demand for members (*e.g.*, columns or beams) with a higher load-carrying capacity led to an increasing usage of built-up members, obtained by connecting two or more CFS profiles by means of discrete fasteners (*e.g.*, Yu *et al.* 2019) – Figure 1 shows a sheathed wall stud system with single and built-up members.

Since CFS built-up members exhibit very slender cross-sections and considerable lengths, features making them highly prone to instability phenomena, their structural efficiency can only be adequately assessed after acquiring in-depth information about their buckling behavior, namely the mechanics involved in local, distortional and global buckling (*e.g.*, Stone & LaBoube 2005 and Rasmussen *et al.* 2020). In addition, the last few years witnessed a fair amount of research work devoted to the development of efficient design rules for CFS built-up members with screw-connected cross-sections. The most relevant fruits of this research

[1] FECFAU, DES, Universidade Estadual de Campinas (UNICAMP), Brazil. <cbasagli@unicamp.br>
[2] CERIS, DECivil, Instituto Superior Técnico, Universidade de Lisboa, Portugal. <dcamotim@ist.utl.pt>
[3] CERIS, Universidade NOVA de Lisboa, Caparica, Portugal. <rodrigo.goncalves@fct.unl.pt>

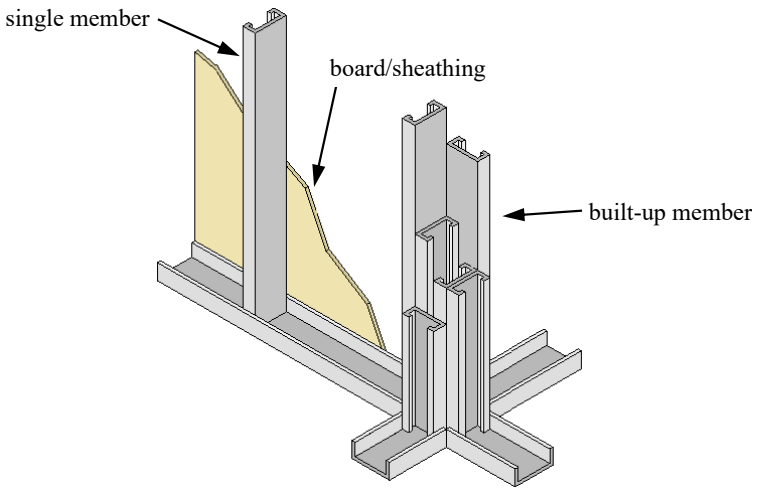

Figure 1: Sheathed wall stud system with single and built-up CFS members.

activity consist of design procedures based on the Direct Strength Method (DSM), nowadays widely accepted as the most efficient approach to design CFS members (*e.g.*, columns or beams) – the prediction of the member load-carrying capacity is based solely on its elastic buckling and yield stresses. The design procedures reported by Fratamico *et al.* (2018a,b), Georgieva *et al.* (2012), Vy *et al.* (2021), Selvaraj & Madhavan (2022) and Li & Young (2023) deserve to be mentioned.

Since the DSM-based design of a CFS built-up member requires the knowledge of its local, distortional and/or global buckling stresses, it is essential to equip practitioners with easily accessible, computationally efficient and user-friendly numerical tools to calculate them accurately. Therefore, the development and wide dissemination of such numerical tools is mandatory before the codification of design specifications. This is why several researchers have recently reported computer programs, based on the Finite Strip Method (FSM), to perform the buckling analysis of CFS built-up members. Among them, it is worth mentioning (i) Fratamico & Schafer (2014), who used nodal multi-point constraints to tie translational degrees-of-freedom belonging to adjacent plate strips (continuously along the member length) and (ii) Li & Young (2022), who considered "solid strips" at the fastener locations (with widths equal to their diameters) – it should be noted that these two approaches assume longitudinally continuous fasteners. In order to overcome the above limitation, Abassi *et al.* (2018) and Mahar & Jayachandran (2020) employed the Compound Finite Strip Method (Puckett & Gutkowski 1986) and incorporated the stiffness properties of the discrete fasteners (obtained from standard beam theory) into the finite strip stiffness matrices. Very recently, Khezri & Rasmussen (2023) improved the formulation of Abassi *et al.* (2018), by including of a methodology to decompose the built-up member buckling modes into linear combinations of structurally meaningful "deformation modes", thus enabling a better grasp of their mechanical natures.

One possible alternative to the above approaches is the use of a buckling formulation based on Generalized Beam Theory (GBT), an approach to the analysis of thon-walled members and structural systems that has been significantly enhanced in the last few years (*e.g.*, Camotim *et al.* 2022 and Gonçalves *et al.* 2023). However, an important gap needs to be bridged before a meaningful GBT-based approach can be employed to analyze thin-walled members with built-up cross-sections: it is indispensable to be able to handle the displacement and rotation compatibility at the fastener locations, corresponding to cross-section mid-line points (longitudinally) spaced along the built-up member length, while retaining the GBT unique "modal language".

The objective of this work is to present and discuss the available results of an ongoing investigation on the development and application of GBT to analyze the buckling behavior of CFS built-up members with longitudinally discrete fasteners. Initially, the formulation of a beam finite element is described, with particular emphasis on the procedures involved in determining the built-up member linear and geometric stiffness matrices. The finite element accounts for the presence of the discrete fasteners by means of constraint equations involving the displacements and rotations of the linked points belonging to each individual profile – this approach constitutes a first step towards more realistic fastener simulations. Then, in order to illustrate the application and potential of the proposed GBT-based approach, numerical results concerning the global, distortional and local buckling behavior of built-up columns, formed by two or three lipped channel profiles connected by discrete fasteners with several longitudinal spacing values, are presented and discussed. Due to the GBT unique modal nature, it is possible to unveil mechanical aspects involved in the various built-up column instability phenomena dealt with. For validation purposes, most of the GBT results obtained are compared with values yielded by accurate ("exact") ANSYS shell finite element analyses that also simulate the discrete fastener influence solely by means of constraint equation.

2. GBT Formulation for the Buckling Analysis of Built-Up Members

Since all available GBT formulations and applications to cold-formed steel structures involve exclusively members with single cross-sections, the development of a GBT-based formulation capable of handling built-up members connected by discrete fasteners must be able to ensure displacement and rotation compatibility at the various fastener locations along the member length, while still retaining the GBT unique modal language. Developing a GBT formulation that achieves this goal is the purpose of this section. However, and as mentioned earlier, the authors are fully aware that such a formulation constitutes only a first step in the path towards reaching a more realistic simulation of the fastener influence, indispensable to obtain a robust GBT-based formulation to perform buckling analyses of built-up members. Further developments, planned for the near future, must necessarily include the incorporation of several aspects such as the (i) fastener geometry and stiffness, (ii) gaps between the connected walls, (iii) wall localized flexibility (governing the crushing phenomenon in the close vicinity of the fastener locations) and (iv) unilateral contact between the walls – *e.g.*, Abassi *et al.* (2018) and Mahar & Jayachandran (2020).

Since the cross-section displacement field is expressed as a linear combination of structurally meaningful deformation modes, GBT analyses involve solving equilibrium equations written in a very convenient and clarifying modal form, leading to solutions that provide in-depth insight on the mechanics of the structural response under consideration. When analyzing the buckling behavior of a built-up member (*i.e.*, solving the eigenvalue problem providing its buckling loads and mode shapes), it is necessary to begin by performing preliminary cross-section analyses (*e.g.*, Bebiano *et al* 2015) of all the individual profiles forming the built-up member. They lead to (i) the identification of the various deformation mode sets and (ii) the evaluation of the associated modal mechanical properties.

Figure 2 depicts an arbitrary prismatic built-up member formed by two generic CFS profiles (1 and 2) connected by discrete fasteners linking the (mid-surface) points (i) P_A^1 and P_A^2, and (ii) P_B^1 and P_B^2, belonging to the GBT discretizations of two longitudinally spaced cross-sections. The local coordinate axes *x*, *s*, *z* associated with each wall (note that coordinate *s* is along the cross-section mid-line) are also shown in Figure 2. In a GBT formulation, member wall mid-plane displacement components (*u*, *v*, *w*) of an individual profile are expressed as

$$u(x,s) = u_k(s)\varphi_{k,x}(x) \qquad v(x,s) = v_k(s)\varphi_k(x) \qquad w(x,s) = w_k(s)\varphi_k(x) \quad , \quad (1)$$

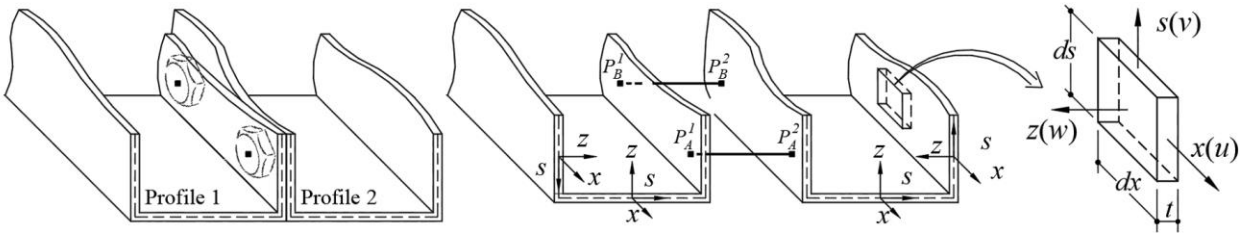

Figure 2: Arbitrary prismatic thin-walled built-up member formed by two individual profiles (1 and 2) and connected by two fasteners, located at points A and B, and wall local coordinate axes (displacement components).

where (i) $(.)_{,x} \equiv d(.)/dx$, (ii) the summation convention applies to subscript k, (iii) functions $u_k(s)$, $v_k(s)$ and $w_k(s)$, yielded by the cross-section analysis, characterize the member cross-section deformation mode k and (iv) $\varphi_k(x)$ is the respective deformation mode amplitude function, defined along the member length.

In order to establish the member equilibrium equation system defining the buckling eigenvalue problem, one impose the adjacent equilibrium condition

$$\delta \mathrm{U}(\Delta\varphi_k) = 0 \quad , \quad (2)$$

expressed in terms of the strain energy variation associated to the configuration change of $\Delta\varphi_k$ (from the underformed state, located on the fundamental equilibrium path), where δ denotes a virtual variation. The strain energy variation of an individual profile (δU) is given by the sum of a linear or material term (Δ is dropped for the sake of conciseness),

$$\int_L \left(C_{ik}\varphi_{k,xx}\delta\varphi_{i,xx} + {}^1D_{ik}\varphi_{k,x}\delta\varphi_{i,x} + {}^2D_{ik}\varphi_k\delta\varphi_{i,xx} + {}^2D_{ki}\varphi_{k,xx}\delta\varphi_i + B_{ik}\varphi_k\delta\varphi_i \right) dx \quad , \quad (3)$$

and a non-linear or geometric term,

$$\lambda \int_L W_j^0 X_{jik}\, \varphi_{k,x}\delta\varphi_{i,x}\, dx \quad , \quad (4)$$

where (i) L is the profile/member length, (ii) C_{ik}, ${}^1D_{ik}$, ${}^2D_{ik}$ and B_{ik} are GBT linear modal matrices, (iii) λ is the load parameter, (iv) W_j^0 is a vector whose components j are the normal stress resultants and (v) X_{jik} are the associated GBT geometric modal matrices – expressions providing all these matrix components can be found in the work of Bebiano *et al* (2015).

The built-up member bucking analysis is performed by means of a GBT-based beam (one-dimensional) finite element with length L_e whose degrees of freedom (*dof*) are the nodal values and derivatives of the GBT deformation mode amplitude functions concerning all the individual profiles (1 and 2, in the illustrative case depicted in Fig. 2) – the deformation modes included in the analysis, which are obtained through the cross-section analyses of the individual profiles, exhibit different natures, namely (i) global (cross-section in-plane rigid-body motions: axial extension, major/minor axis bending and torsion), (ii) distortional, (iii) local and (iv) shear (membrane type) (see Bebiano *et al* 2015). The modal amplitude functions of each individual profile ($\varphi_k^1(x)$ and $\varphi_k^2(x)$ in this case) are approximated by means of linear combinations of standard Hermite cubic polynomials, *i.e.*,

$$\varphi_k(x) = d_{k.1}^e\psi_1(\xi) + d_{k.2}^e\psi_2(\xi) + d_{k.3}^e\psi_3(\xi) + d_{4.1}^e\psi_4(\xi) \quad , \quad (5)$$

where $d^e_{k.1} = \varphi_{k,x}(0)$, $d^e_{k.2} = \varphi_k(0)$, $d^e_{k.3} = \varphi_{k,x}(L_e)$, $d^e_{k.4} = \varphi_k(L_e)$ are the finite element generalized displacements, $\xi = x/L_e$ and

$$\psi_1 = L_e(\xi^3 - 2\xi^2 + \xi) \quad \psi_2 = 2\xi^3 - 3\xi^2 + 1 \quad \psi_3 = L_e(\xi^3 - \xi^2) \quad \psi_4 = -2\xi^3 - 3\xi^2 \quad . \quad (6)$$

Incorporating (5) and (6) into (2) and carrying out the appropriate integrations, the individual profile finite element linear ($[K]^e$) and geometric ($[G]^e$) stiffness matrices are obtained. The overall individual profile linear ($[K]$) and geometric ($[G]$) stiffness matrices are determined by assembling their finite element counterparts. In the case of the illustrative built-up member considered here, depicted in Figure 2 and formed by two individual profiles (1 and 2), the linear ($[\mathrm{K}]^{1+2}$) and geometric ($[\mathrm{G}]^{1+2}$) matrices combine the individual profile ones ($[\mathrm{K}]^1$, $[\mathrm{G}]^1$, $[\mathrm{K}]^2$, $[\mathrm{G}]^2$), but taking into account the constraints that need to be enforced to simulate the presence of the two fasteners – they ensure the displacement and rotation compatibility at the individual profile mid-surface points linked by the fasteners.

In order to illustrate the establishment of the above constraint/compatibility conditions, consider the fastener (*e.g.*, a self-tapping screw) shown in Figure 3, which link two points (R^m and R^n) located in a the mid-lines of the cross-section of a built-up member formed by two connected individual profiles (*m* and *n*), respectively at coordinates s^m_R and s^n_R. First of all, GBT intermediate nodes must be placed at the points R^m (on the profile *m* cross-section mid-line) and R^n (on the profile *n* cross-section mid-line). Then, constraining all nodal translations and rotations (except the drill rotation) at the common point *R* requires enforcing the compatibility conditions involving the displacements and rotations associated with the individual profile GBT deformation modes included in the analysis, which read

$$u^m_k(s^m_R)\varphi^m_{k,x}(x_R) = u^n_k(s^n_R)\varphi^n_{k,x}(x_R) \quad (7)$$

$$v^m_k(s^m_R)\varphi^m_k(x_R) = v^n_k(s^n_R)\varphi^n_k(x_R) \quad (8)$$

$$w^m_k(s^m_R)\varphi^m_k(x_R) = w^n_k(s^n_R)\varphi^n_k(x_R) \quad (9)$$

$$w^m_{k,s}(s^m_R)\varphi^m_k(x_R) = w^n_{k,s}(s^n_R)\varphi^n_k(x_R) \quad (10)$$

$$w^m_k(s^m_R)\varphi^m_{k,x}(x_R) = w^n_k(s^n_R)\varphi^n_{k,x}(x_R) \quad , \quad (11)$$

where a null distance between the two points is assumed (the generalization to finite distances, associated with gaps between the connects walls, will be addressed in the near future). After performing the above

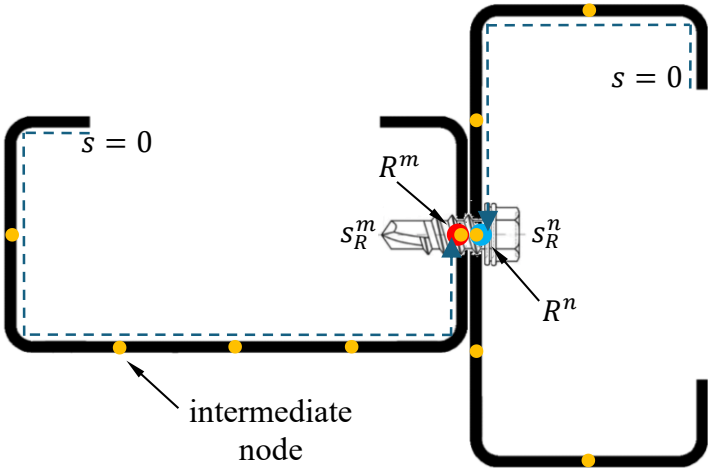

Figure 3: Displacement and rotation compatibility at points R^m and R^n of two profiles forming a built-up member.

procedure for all the built-up member discrete fasteners (in all connected cross-sections along the member length), the full set of constraint equations can be expressed, in matrix form, as

$$\{d\} = [\Omega]\{\tilde{d}\} \quad . \quad (12)$$

where (i) $\{d\}$ is the generalized mode displacement vector, (ii) $[\Omega]$ is the compatibility matrix, containing the deformation mode displacement and rotation values at the full set of individual profile connected points, and (iii) $\{\tilde{d}\}$ is the "constrained generalized mode displacement vector" at those same points, which takes into account the displacement and rotation compatibility. After knowing matrix $[\Omega]$, the displacement and rotation compatibility at the fastener locations is imposed on the built-up member linear and geometric stiffness matrices through a condensation operation. In the case of the illustrative example depicted in Figure 2, which concerns a built-up member formed by two individual profiles (1 and 2) connected by two fasteners (A and B, located in different cross-sections), this operation reads

$$\begin{bmatrix} [\tilde{K}]^1 & 0 \\ 0 & [\tilde{K}]^2 \end{bmatrix} + \lambda \begin{bmatrix} [\tilde{G}]^1 & 0 \\ 0 & [\tilde{G}]^2 \end{bmatrix} = [\Omega]^T \begin{bmatrix} [G]^1 & 0 \\ 0 & [G]^2 \end{bmatrix} [\Omega] + \lambda [\Omega]^T \begin{bmatrix} [G]^1 & 0 \\ 0 & [G]^2 \end{bmatrix} [\Omega] \quad , \quad (13)$$

where the compatibility matrix $[\Omega]$ containing the deformation mode displacement values at the mid-line coordinates $s_A^1 \equiv s_B^1$ and $s_A^2 \equiv s_B^2$ of the cross-sections at the longitudinal coordinates x_A and x_B (the fastener locations are the same at the two connected cross-sections). Since (i) the buckling eigenvalue problem defined by (13) is written in terms of the generalized vector $\{\tilde{d}\}$ components and, for the sake of structural clarity, (ii) it is convenient/desirable to achieve a fully modal solution, expressed in terms of the GBT deformation modes of all individual profiles, it is necessary to revert again to the "unconstrained generalized mode displacement vector", which requires performing the operation defined by (12) (*i.e.*, $\{\tilde{d}\} \Rightarrow \{d\}$).

3. Illustrative Examples

In order to illustrate the application and capabilities of the proposed GBT-based buckling formulation, numerical results concerning the flexural, flexural-torsional, local and distortional buckling of simply

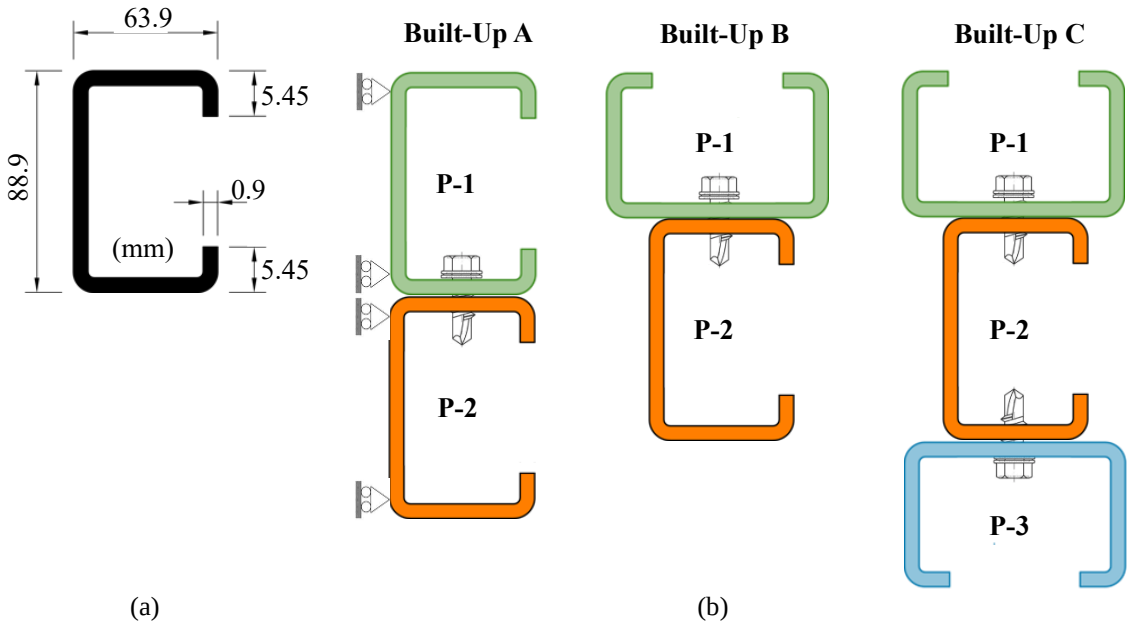

Figure 4: (a) Lipped channel dimensions and (b) built-up column cross-section and fastener locations considered in this work.

supported built-up columns (uniformly compressed members) formed by two or three identical lipped channel profiles (i) made of steel with E=210 *GPa* (Young's modulus) and ν=0.3 (Poisson's ratio), (ii) with the cross-section dimensions given in Figure 4(a) and (iii) connected by discrete fasteners. Figure 4(b) shows the built-up column cross-section configurations and fastener locations considered, termed "Built-Up A", "Built-Up B" and "Built-Up C", respectively – in each case, various fastener longitudinal spacing values are dealt with. For validation and comparison purposes, most of the GBT-based results obtained are compared with values obtained by means of (i) accurate ("exact") ANSYS (SAS 2013) shell finite element (SFEA) and (ii) CUFSM (*e.g.*, Li & Schafer 2010) finite strip analyses – the latter concern built-up columns formed by continuously connected individual profiles (a master-slave approach is adopted to tie their translational and rotational degrees of freedom).

Figure 5 concerns the lipped channel deformation modes employed in the GBT buckling analysis performed in this work – it displays the (i) in-plane shapes of the (rigid-body, distortional and local) conventional modes (except for mode **1** – axial extension) and (ii) the out-of-plane (warping) shapes of the shear modes (Bebiano *et al* 2015). These deformation modes correspond to a lipped channel discretization involving nine intermediate nodes (three in the web and each flange). For subsequent

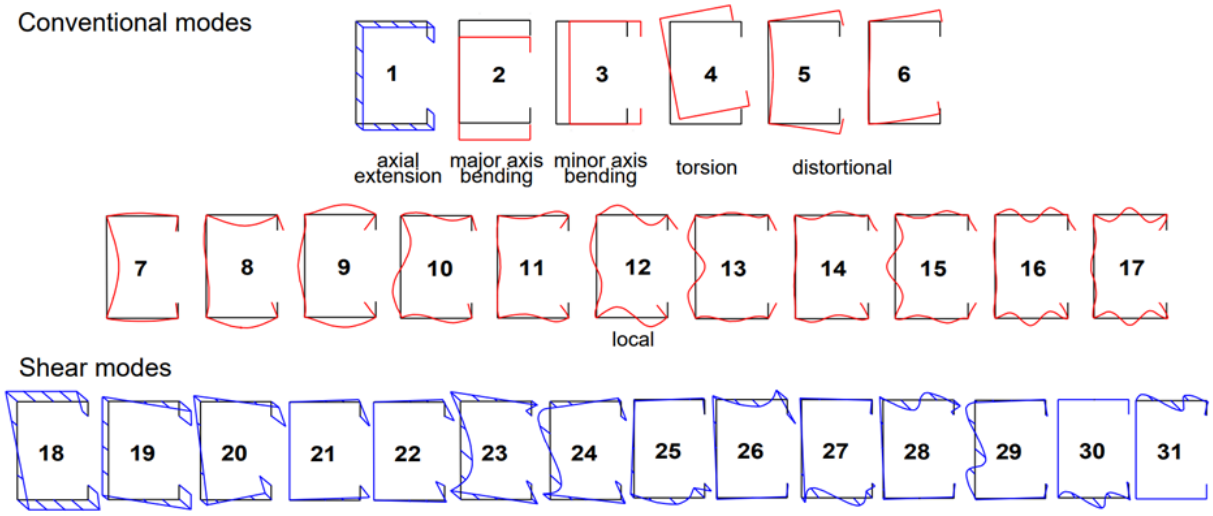

Figure 5: GBT conventional (in-plane) and shear (out-of-plane) lipped channel deformation mode shapes.

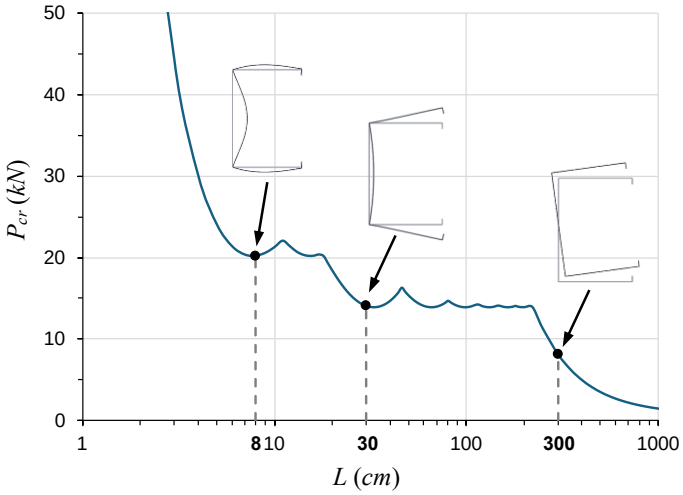

Figure 6: Signature curve (P_{cr} vs. L) of the simply supported uniformly compressed individual lipped channel profile.

comparison purposes, Figure 6 shows the signature curve (variation of the critical buckling load P_{cr} with the length L) of the simply supported uniformly compressed individual profile – also shown are the local, distortional and flexural-torsional critical buckling mode shapes (occurring for the lengths indicated).

3.1 Flexural buckling

Initially, the influence of the fastener spacing on the major-axis flexural buckling of laterally restrained columns with the Built-Up A cross-section and length L=240 *cm* is investigated – therefore, only the axial extension (**1**), major-axis bending (**2**) and shear (**18**-**31**) modes are included in the GBT analyses. Table 1 provides, for different fastener spacing values ($\mathbb{s}$), column critical buckling loads (P_{cr}) obtained by means of (i) ANSYS SFEA ("exact" values, for validation purposes) and (ii) two GBT analyses, one including only the conventional (rigid-body) deformation modes **1** and **2**, and the other including also the 14 shear deformation modes – the Δ (%) values provide the differences with respect to the "exact" critical buckling loads. Figures 7(a)-(b) depict the GBT modal amplitude functions and/or their derivatives concerning the critically buckled shapes of the built-up column individual profiles **P-1** and **P-2**, for a fastener spacing $\mathbb{s}$=60 *cm*. Figure 8(a) shows an ANSYS 3D view of the $\mathbb{s}$=120 *cm* column buckled end support region, including a fastener detail, whereas Figure 8(b) displays the warping (axial) displacement amplitudes $\bar{u}$ along the column end-section overall (double) web, for $\mathbb{s}$=120; 60; 10 *cm*. The observation of the results presented in these table and figures prompts the following remarks:

(i) First of all, the buckling loads yielded by the ANSYS and the GBT buckling analyses including the shear modes virtually coincide – all differences are below 2.4%. In addition, note that the influence of the shear modes grows with the fastener spacing and becomes meaningful for $\mathbb{s}$>40 *cm*, in the sense that removing them from the GBT analyses leads to differences above 5%.

(ii) Besides the warping displacements associated with mode **2** ($\varphi_{2,x}$), the inclusion of mode **1** ($\varphi_{1,x}$) in the GBT analysis is indispensable to enable the capture the horizontal centroid shift between the built-up column and individual profile cross-sections. On the other hand, including the shear modes, whose modal amplitude functions are shown in Figure 7(b), makes it possible to capture the variation of the warping displacements along the connected flange regions (see Figs. 8(a)-(b)).

(iii) The comparison between the three warping displacement curves shown in Figure 8(b) shows that the behavior of the $\mathbb{s}$=10 *cm* built-up column is very close to that of a column with a single cross-section combining the two lipped channels. Besides the fact that the warping displacement is practically null at the common flange, the critical buckling loads of the two columns are practically identical (the value obtained with the Euler formula is 486.64 *kN*).

Table 1: ANSYS and GBT Built-Up A column member critical buckling loads.

Spacing	SFEA	GBT (**1**+**2**)		GBT (**1**+**2**+**Shear**)	
$\mathbb{s}$ (*cm*)	P_{cr} (*kN*)	P_{cr} (*kN*)	Δ (%)	P_{cr} (*kN*)	Δ (%)
120	358.97	381.72	6.3	361.12	0.6
80	403.80	433.38	7.3	409.52	1.4
60	427.16	455.12	6.5	431.89	1.1
40	450.32	472.16	4.8	450.73	0.1
30	461.47	478.46	3.7	459.50	-0.4
20	472.05	483.07	2.3	465.50	-1.4
10	481.68	485.89	0.9	470.23	-2.4

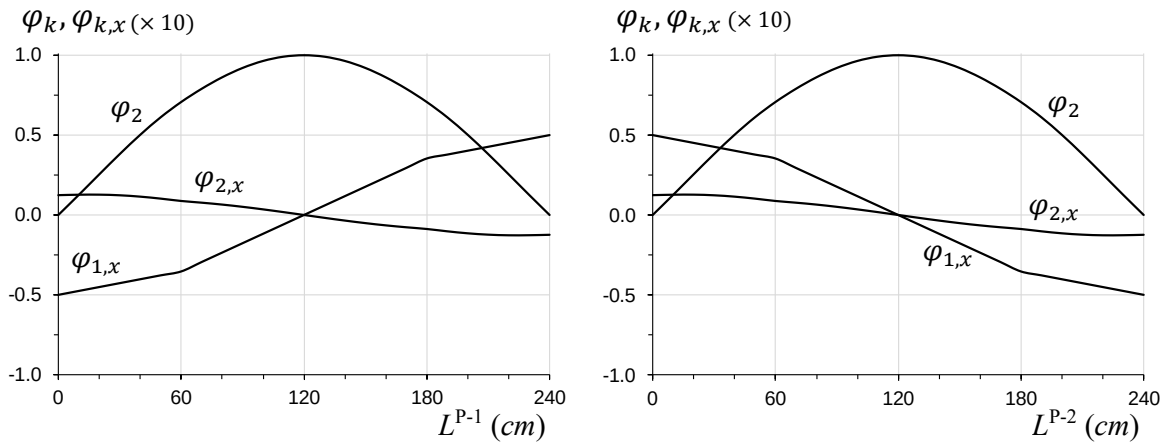

(a)

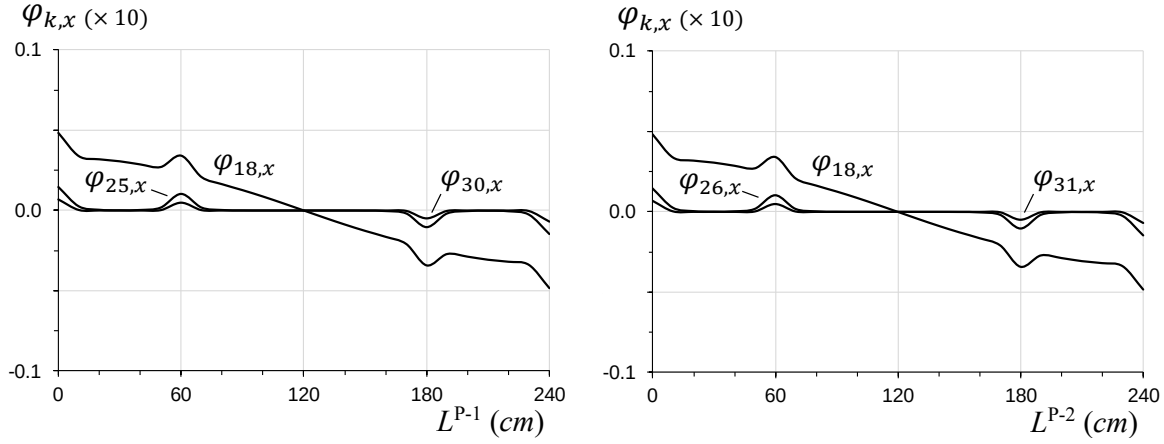

(b)

Figure 7: Modal amplitude functions of the critically buckled built-up column individual profiles, $\mathbb{s}$=60 *cm*: (a) conventional and (b) shear modes.

3.2 Flexural-torsional buckling

Attention is now turned to assessing the influence of the fastener spacing on the flexural-torsional buckling behavior of columns with the Built-Up B cross-section, length L=300 *cm* and three fastener spacing values ($\mathbb{s}$=150; 75; 37.5 *cm*). Table 2 provides the column critical buckling loads (P_{cr}) obtained by means of the ANSYS SFEA ("exact" values) and GBT-based analyses – in the latter case, including either all (shear and conventional) deformation modes or only the conventional ones. Figure 9 displays the most relevant modal amplitude functions participating in the critically buckled shapes of the two individual profiles, whereas Figure 10 provides the 3D representations of the corresponding built-up column critical buckling modes yielded by the ANSYS SFEA – for the sake of clarity, only the deformed edges are shown. The observation of these GBT-based and ANSYS buckling results prompts the following remarks:

(i) Once again, there is a very good correlation between the GBT and ANSYS critical buckling loads. Concerning the critical buckling load accuracy improvement achieved by including the shear modes in the GBT analysis, the percentage differences with respect to the "exact" values decrease by about 20% (the maximum one drops from 4.4% to 3.5% – see Table 2).

(ii) Decreasing the fastener spacing from $\mathbb{s}$=150 *cm* to $\mathbb{s}$=37.5 *cm* leads to a built-up column buckling load increase of around 10%.

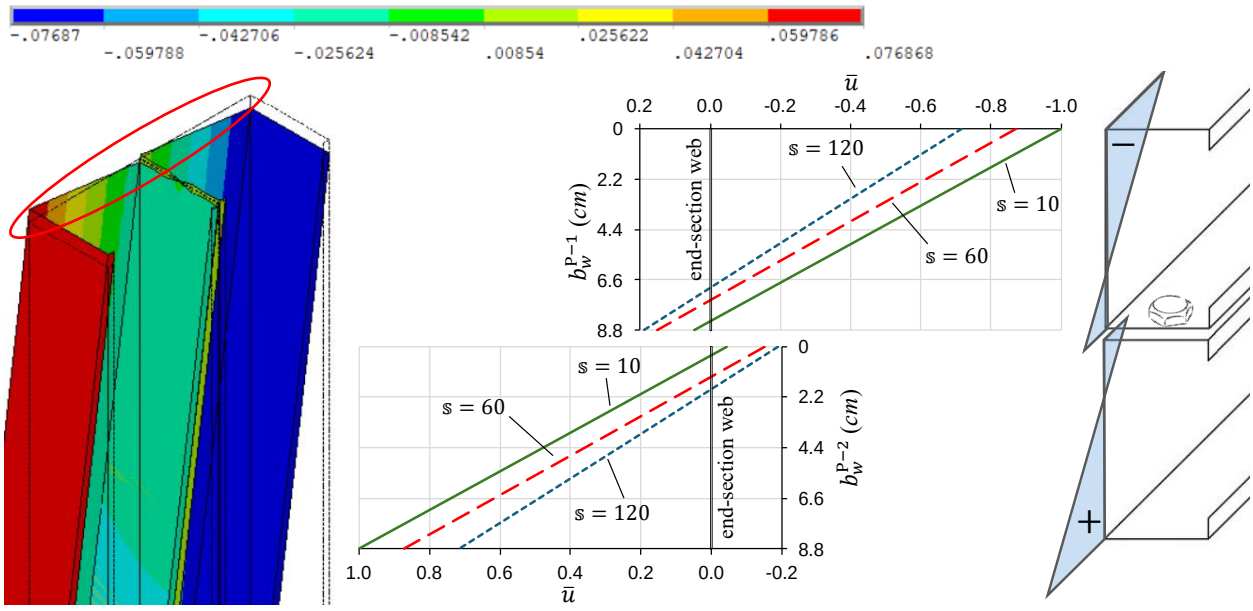

(a) (b)

Figure 8: (a) ANSYS 3D view of the 𝕤=120 *cm* column buckled end support region and (b) warping displacement amplitudes along the column end-section overall (double) web, for 𝕤=120; 60; 10 *cm*.

Table 2: ANSYS and GBT critical buckling loads for the columns with Built-Up B cross-section and length L=300 cm.

Spacing	SFEA	GBT (**1-17** modes)		GBT (**1-17**+**18-31** modes)	
𝕤 (*cm*)	P_{cr} (*kN*)	P_{cr} (*kN*)	Δ (%)	P_{cr} (*kN*)	Δ (%)
150	22.04	23.01	4.4	22.82	3.5
75	23.15	24.04	3.9	23.85	3.0
37.5	24.41	25.06	2.7	24.93	2.1

(iii) Before addressing the modal amplitude functions shown in Figure 9, it is worth recalling that they are displayed in the "modal language" pertaining to each individual profile (see Fig. 5). For instance, for the cross-section orientation displayed in Fig. 4(b) mode **2** (major-axis flexure) corresponds to a horizontal translation of profile **P-1** and to a vertical translation of profile **P-2** (conversely for the minor-axis flexural mode **3**). Moreover, it also noted that, even if the built-up column cross-section has no symmetry, its major and minor axes are "almost horizontal" and "almost vertical", respectively (slight clockwise rotation from the horizontal and vertical axes).

(iv) There is a very close agreement between the modal amplitude functions shown in Figure 9 and the corresponding buckling mode shapes represented in Figure 10. However, the former provide deeper insight on the influence of the fastener spacing on the mechanics of built-up column buckling. In particular, they enable assessing in detail the variation in the distortional and local deformations, an assessment not feasible through the inspection of buckling mode shapes obtained from shell finite element analyses.

(v) The built-up column critical buckling mode combines global, local and distortional deformation modes in both profiles, even if, as expected, the global ones are clearly dominant. Moreover, and regardless of the fastener spacing, the two profile buckled shapes exhibit quantitatively different modal amplitudes – those concerning profile **P-1** are visibly larger. This difference stems from the fact that the column flexural-torsional buckling associated with the fully connected cross-section combines an

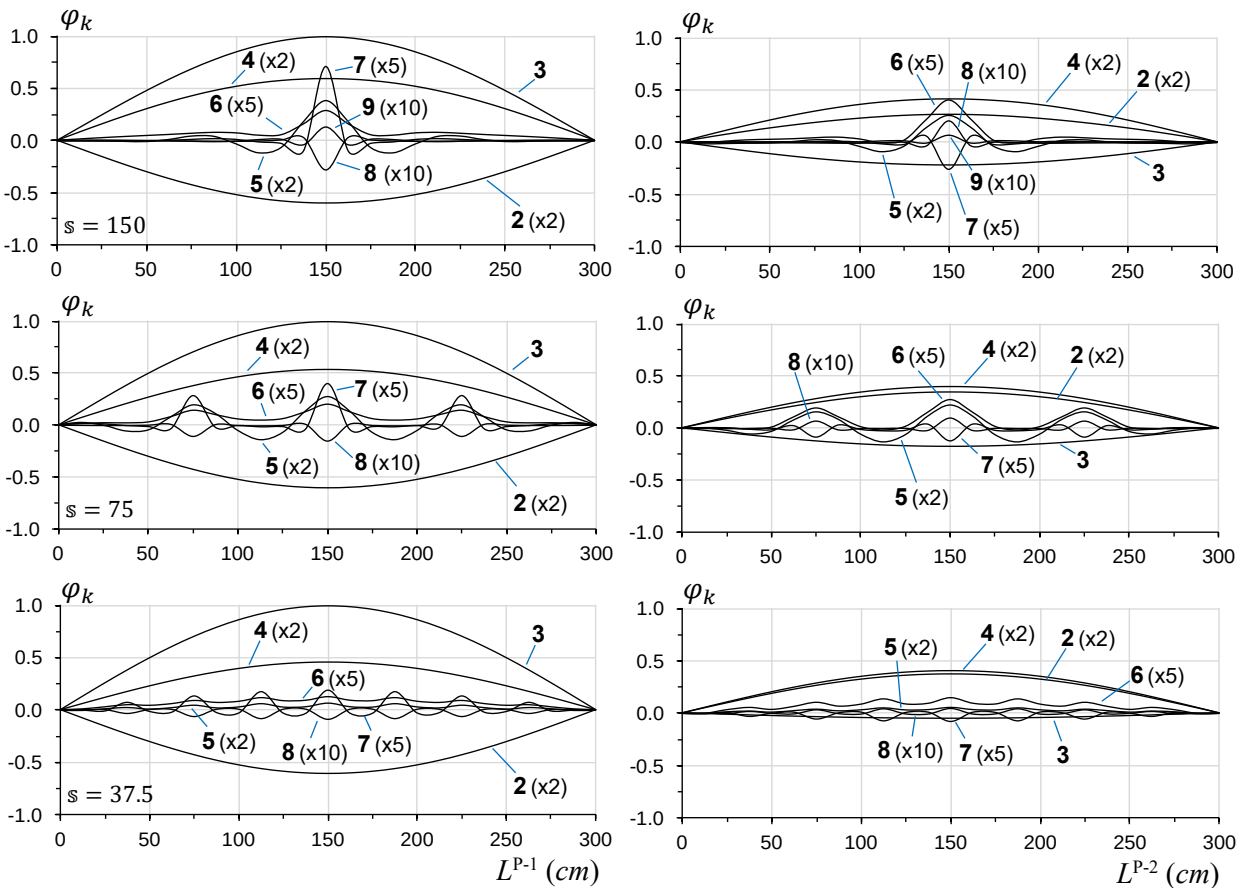

Figure 9: Modal amplitude functions of the columns with the the Built-Up B cross-section and length L=300 *cm*.

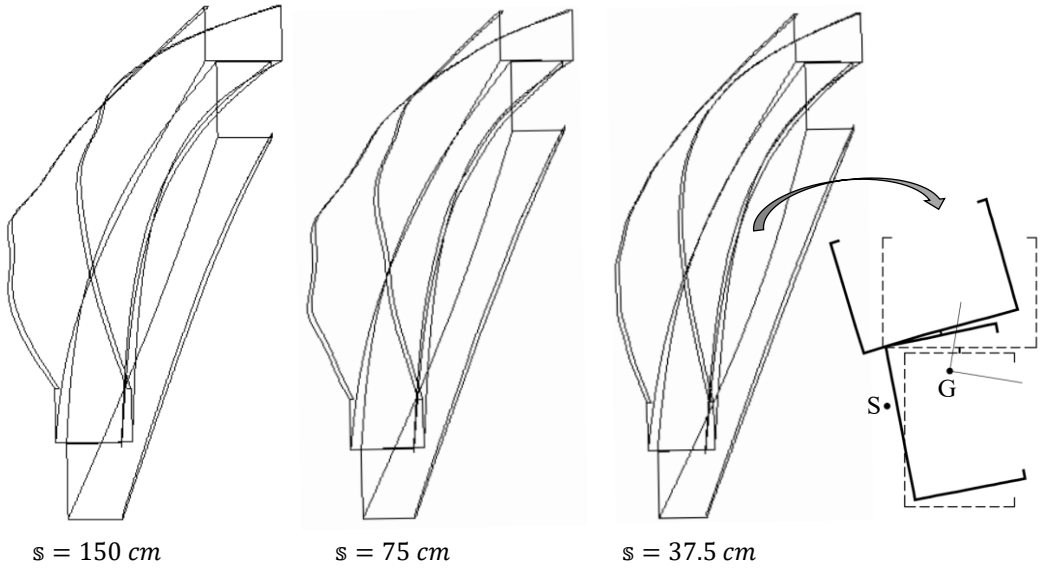

Figure 10: ANSYS critical buckling mode shapes of the columns with the Built-Up B cross-section and length L=300 *cm*.

"almost vertical" translation with a torsional rotation about its shear center, located 1.09 *cm* to the left and 5.56 *cm* above the left bottom corner of the profile **P-2** cross-section (see the right hand side of Fig. 10). Then, the occurrence of fairly large mode **2** and mode **3** amplitudes in profile **P-1** (its cross-

section centroid is located quite far away from the built-up cross-section shear center) is just logical. Conversely, profile **P-2** exhibits moderate mode **2** and small mode **3** amplitudes (the latter become very tiny for s=37.5 *cm* – the built-up and fully connected column buckling behaviors become closer). On the other hand, the torsional rotations are quite similar in both profiles and become almost identical for s=37.5 *cm* (an almost perfect overall rotation compatibility takes place).

(vi) Finally, the participations of the distortional and local deformation modes, appearing due to the need to ensure compatibility at the fastener locations, are only meaningful in the close vicinity of the fastener locations and become smaller as the fastener spacing decreases. Once again, these modal participations are visibly larger in profile **P-1** than in profile **P-2** – this is because of the different fastener locations (mid-points of the web and top flange, respectively). As can be observed in the buckling mode shapes shown in Figure 10, the distortional and local deformations are only perceptible to the naked eye in the buckled profiles **P-1** of the built-up column with s=150 *cm* and s=75 *cm*.

(vii) For comparison purposes, the built-up column critical buckling load provided by the CUFSM finite strip analysis, which assumes longitudinally continuous fasteners, is equal to 25.93 *kN* – 4% above the value obtained GBT for the column with s=37.5 *cm*.

3.3 Distortional buckling

The influence of the fastener spacing on the distortional buckling behavior of columns with the Built-Up B (two profiles) and Built-Up C (three profiles) cross-sections, length L=30 *cm* and two fastener spacing values (s=15; 7.5 *cm*) is addressed in this section. Table 3 compares the critical buckling loads provided by the ANSYS SFE and GBT analyses for the built-up columns with the two cross-sections and two fastener spacing values considered. Figures 11 to 13 provide representations of the corresponding built-up column critical buckling modes, namely (i) the GBT modal amplitude functions of the individual profiles **P-1** and **P-2** (note that, due to the Built-Up C cross-section symmetry with respect to the centroidal horizontal axis, the buckled shapes of profiles **P-1** and **P-3** are identical and, therefore, only the former are shown) and (ii) ANSYS 3D views concerning three (out of four) column buckling modes. The observation of these buckling results leads to the following comments:

(i) Unlike in the previous cases, the GBT analyses including only the conventional deformation modes provide very accurate column critical buckling load estimates – the GBT and ANSYS ("exact") values never differ by more than 3.6%. Moreover, including also the shear deformation modes in the GBT analyses merely drops the differences by no more than 0.3%.

(ii) The influence of the fastener spacing on the critical buckling load is slightly more pronounced in the columns with Built-Up C cross-sections, for which decreasing the fastener spacing (from s=15 *cm* to s=7.5 *cm*) causes a critical buckling load increase of around 5% – in the columns with Built-Up B cross-sections, such increase is only of about 3%.

Table 3: ANSYS and GBT critical buckling loads of columns with Built-Up B + Built-Up C cross-sections and length L=30 *cm*.

Section	Spacing	SFEA	GBT (**1-17** modes)		GBT (**1-17**+**18-31** modes)	
	s (*cm*)	P_{cr} (*kN*)	P_{cr} (*kN*)	Δ (%)	P_{cr} (*kN*)	Δ (%)
Built-Up B	15	29.07	29.79	2.5	29.74	2.3
	7.5	29.86	30.75	3.0	30.69	2.8
Built-Up C	15	43.80	45.07	2.9	44.97	2.7
	7.5	45.84	47.48	3.6	47.35	3.3

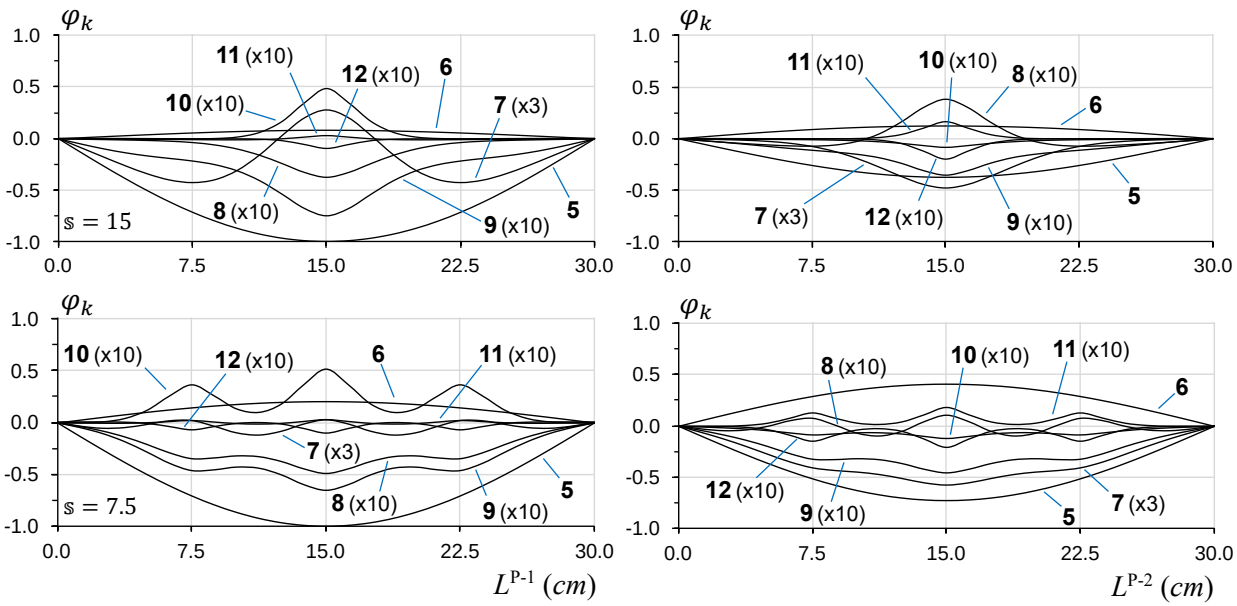

Figure 11: Modal amplitude functions of the columns with the the Built-Up B cross-section and length L=30 *cm*.

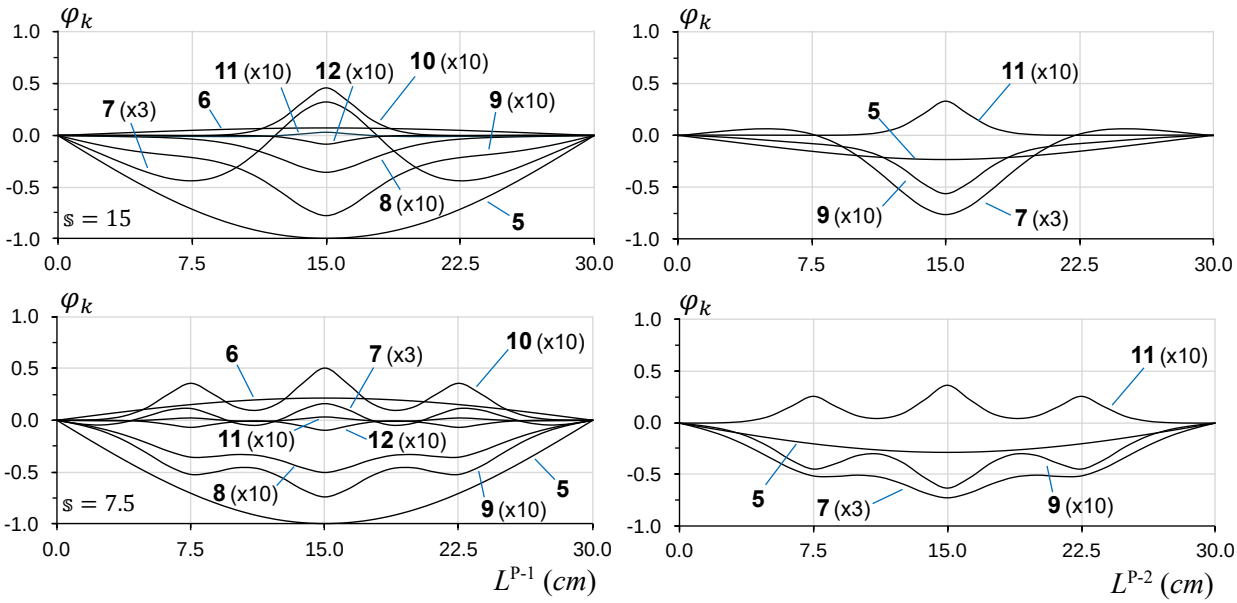

Figure 12: Modal amplitude functions of the columns with the the Built-Up C cross-section and length L=30 *cm*.

(iii) All built-up columns buckle in modes that combine highly dominant distortional deformations with very small local deformations (mostly in the vicinity of the fastener locations). The latter are (iii_1) virtually invisible to the naked eye in the columns with the Built-Up B cross-section and (iii_2) only barely visible near the connected flanges of the columns with the Built-Up C cross-section – this can be attested by just looking at Figure 13 and also by noticing that, with one exception, all local mode amplitude functions in Figures 11 and 12 are amplified 10 times – the exception is the mode **7** one (see Fig. 5), only amplified 3 times. Like in the previous cases, the modal participations are visibly larger (and now also more complex) in profile **P-1** than in **P-2**, particularly in the columns with the Built-Up C cross-section (because there are fasteners in both **P-2** profile flanges) – once again, this fact stems from the different fastener locations in the connected profiles: web mid-point in profile(s) **P-1**

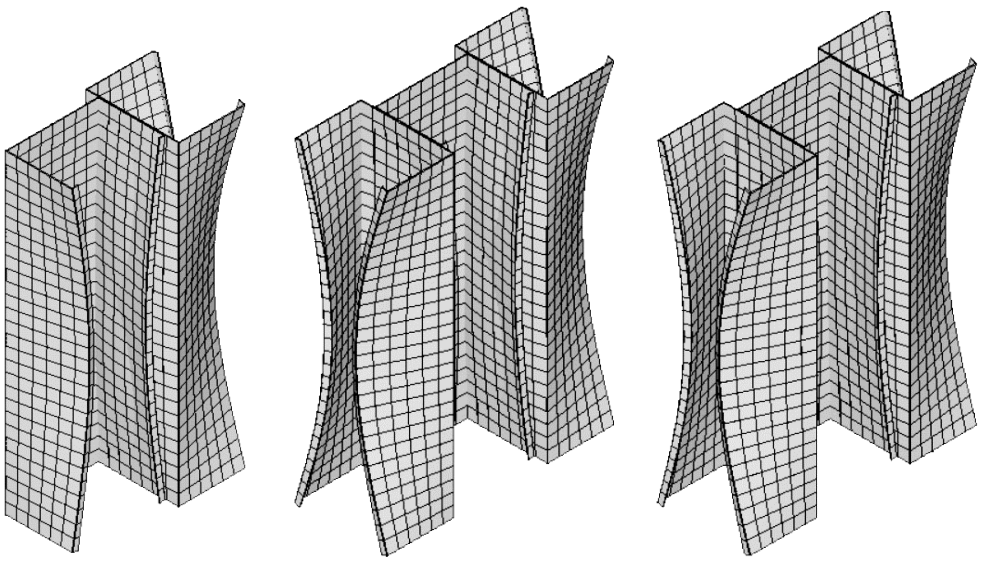

(a) (b)

Figure 13: ANSYS critical buckling mode shapes of columns with L=30 *cm*: (a) column with the Built-Up B and Built-Up C cross-sections and s=15 *cm*, and (b) column with the Built-Up C cross-section and s=7.5 *cm*.

and top/bottom flange mid-point in profile **P-2** – the latter locations are clearly more efficient in restraining the distortional deformations.

(iv) Figures 11 and 12 clearly show that symmetric distortion (mode **5**) is dominant in the buckled shapes of all the individual profiles of the four built-up columns analyzed, which is confirmed by the visual inspection of the three ANSYS 3D views displayed in Figure 13. In the profiles belonging to the columns with the Built-Up B cross-section, there is also a significant participation of anti-symmetric distortion (mode **6**), which stems from the fact that symmetric distortion is restrained by the fasteners – naturally, this restraint is (iv_1) more pronounced in profile **P-2** (more efficient fastener location) and (iv_1) increases as the fastener spacing decreases, which explains why, percentagewise, the presence of mode **6** is more meaningful in profiles **P-2** of the built-up columns with s=7.5 *cm*. The situation is different for the profiles **P-2** belonging to the columns with the Built-Up C cross-section, which stems from its symmetry with respect to the horizontal axis. The buckled shapes of these profiles are fully symmetric, which means that they combine only symmetric deformation modes (**5**+**7**+**9**+**11**) and, thus, anti-symmetric distortion (mode **6**) is absent. Moreover, the local deformation modes (essentially mode **7**) become, percentagewise, much more relevant, as attested by the modal amplitude functions shown on the right side of Figure 12.

(v) The in-depth discussion concerning the column critical buckling mode features, presented in the previous items, was only possible because of the unique modal nature of the GBT analyses – indeed, it would be virtually impossible to acquire such a rich insight on the built-up column buckling mechanics through the ANSYS shell finite element results.

(vi) For comparison purposes, the built-up column critical buckling loads provided by the CUFSM finite strip analyses (assuming longitudinally continuous fasteners) are (vi_1) 31.48 *kN* (column with the Built-Up B cross-section) and (vi_2) 48.88 *kN* (column with the Built-Up C cross-section) – values only slightly above those of the built-up columns with fastener spacing s=7.5 *cm*. Recall also that the critical load of an isolated profile with L=30 *cm* is 14.06 *kN* (see Fig. 6), which means that, in this particular case, the built-up column critical buckling load is 12% (Built-Up B cross-section) and 16% (Built-Up C cross-section) higher than the sum of the individual profile buckling loads.

3.4 Local buckling

Finally, attention is now turned to the assessment of how the fastener spacing influences the local buckling behavior of stub columns with the Built-Up B cross-section, length L=8 *cm* and two fastener spacing values (s=4; 2 *cm* – note that these fastener spacing values are smaller than those typically used in practice). The results presented and discussed here are similar to those reported presented in the previous sections: while Table 4 compares the column critical buckling loads yielded by the ANSYS SFE and GBT-based analyses, Figures 14 and 15 display the modal amplitude functions associated with the critical buckling modes and the corresponding ANSYS 3D representations. After observing all these buckling results, the following conclusions may be drawn:

(i) As already found for distortional buckling (but to an even larger extent), the inclusion of the shear deformations modes in the GBT analyses has virtually no impact: the column critical buckling load estimates obtained are practically identical and very accurate – the GBT and ANSYS values never differ by more than 2.2%. Moreover, Figure 14 shows that the symmetric local deformation mode **7** plays a dominant role in the buckled shapes of both individual profiles in the two built-up columns analyzed – note that all the remaining three modal amplitude functions and heavily amplified.

(ii) Figure 14 also clearly shows that the built-up column local instability is triggered by profile **P-2**, which stems from the fact that its web (the wall driving the instability) is not connected/restrained – note how its modal amplitude functions are visibly larger than their counterparts from profile **P-1**, which is further confirmed by the visual inspection of Figure 15.

Table 4: ANSYS and GBT critical buckling loads of columns with Built-Up B cross-section and length L=8 *cm*.

Section	Spacing	SFEA	GBT (**1**-**17** modes)		GBT (**1**-**17**+**18**-**31** modes)	
	s (*cm*)	P_{cr} (*kN*)	P_{cr} (*kN*)	Δ (%)	P_{cr} (*kN*)	Δ (%)
Built-Up B	4	39.85	40.72	2.2	40.71	2.1
	2	39.86	40.74	2.2	40.72	2.1

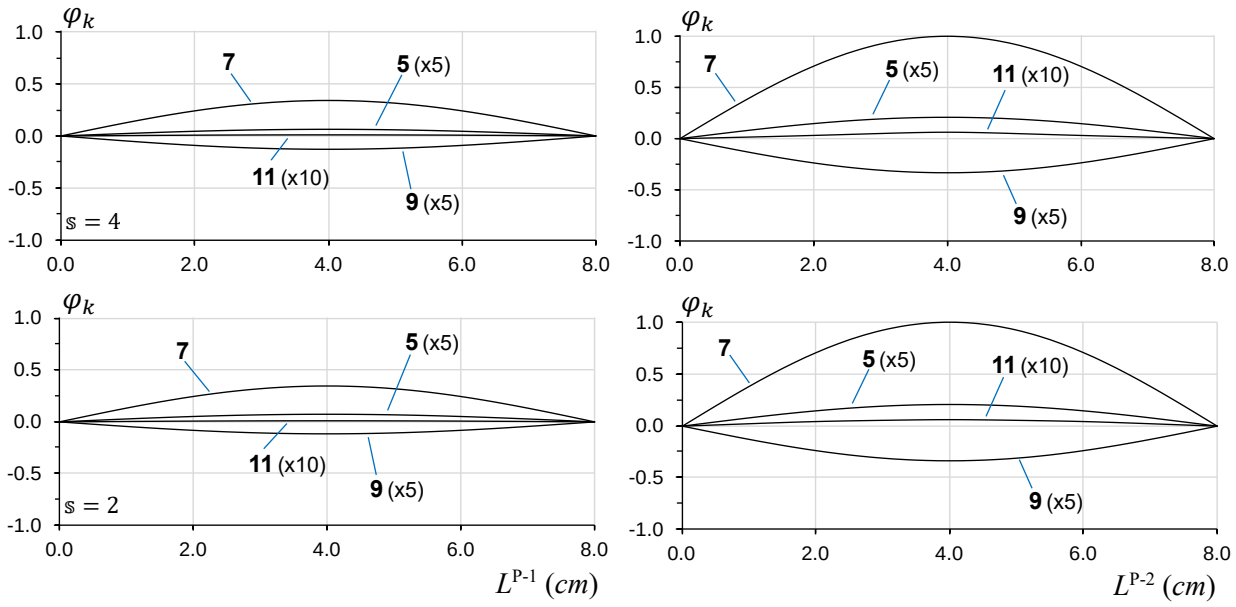

Figure 14: Modal amplitude functions of the columns with the the Built-Up B cross-section and length L=8 *cm*.

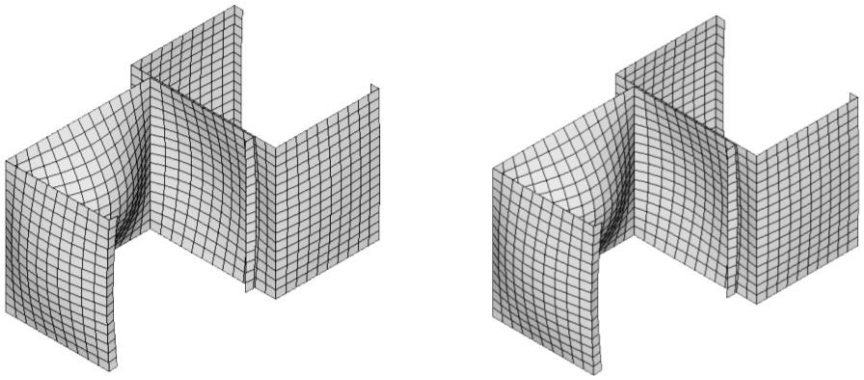

(a) (b)

Figure 15: ANSYS buckling modes of columns with the Built-Up B cross-section, L=8 *cm* and (a) s=4 *cm*, and (b) s=2 *cm*.

(iii) The built-up column critical local buckling load and associated mode shape literally unaffected by the fastener spacing. Moreover, the presence of the fasteners (regardless of the spacing) also has a minute influence, as attested by the fact that the critical local buckling of an isolated profile with L=8 *cm* is 20.23 *kN* (see Fig. 6), *i.e.*, just very slightly below one half of the built-up column value, which is in agreement with the fact that only an extremely small participation of anti-symmetric deformation modes (**6**, **8**, **10**) was detected in the profile **P-2** buckled configuration.

(iv) Finally, for comparison purposes, note that the built-up column critical local buckling load provided by the CUFSM finite strip analysis (assuming longitudinally continuous fasteners) is 40.42 *kN*.

4. Concluding Remarks

This paper reported the available results of an ongoing investigation on the use of GBT to analyze the buckling behavior of cold-formed steel built-up members connected by discrete fasteners. The first step of this investigation consisted of formulating a GBT-based finite element that accounts for the presence of the discrete fasteners by means of constraint equations – it leads to a simple numerical implementation, while retaining the GBT unique modal language. Then, in order to illustrate the application and potential of the proposed GBT formulation, a number of numerical results were presented and discussed – they dealt with the flexural, flexural-torsional, distortional and local buckling behavior of simply supported built-up columns formed by two or three identical lipped channel profiles connected by fasteners with different spacing values. For validation and assessment purposes, most GBT-based buckling results were compared with values yielded by refined ANSYS (shell finite element) and CUFSM (finite strip) analyses, also modeling the fasteners through constraint equations – an excellent agreement was invariably found.

At this stage, it is worth noting that the above GBT formulation was applied in this work exclusively to uniformly compressed built-up members. In the case of built-up members acted by arbitrary loadings, such as those involving end moments or transverse forces, its application becomes slightly more complex, due to the need to determine accurately the member pre-buckling stress state. This can only be achieved by means of preliminary GBT-based linear analyses (i) capable of capturing pre-buckling shear and transverse normal stresses, *i.e.*, including shear and transverse extension deformation modes, and (ii) accounting for the possibility of slip occurring between the connected walls. The authors are currently working on a GBT-based finite element formulation able to perform this task.

Finally, it must also be mentioned that, even if the approach adopted in this work to incorporate the presence of the discrete fasteners in the GBT leads to a rather straightforward numerical implementation

and seems to yield quite reasonable built-up member buckling load estimates, the authors are fully aware that their quality can be improved by considering more realistic (and sophisticated) simulations of the fastener influence. Such simulations must enable incorporating several aspects in the GBT analyses, namely (i) the fastener geometry and stiffness, (ii) the gaps between the connected walls, (iii) the wall localized flexibility/crushing phenomenon near the fastener locations and (iv) the possible occurrence of unilateral contact between adjacent connected walls. Work is under way to incorporate the above effects in the GBT formulation presented in this study – hopefully, the fruits of such research effort will be reported in the not too distant future.

Acknowledgments

The first author gratefully acknowledges the financial support provided by "Conselho Nacional de Desenvolvimento Científico e Tecnológico" (CNPq – Ministry of Science, Technology and Innovation of Brazil), through project n◦ 307640/2022-1. The second and third authors gratefully acknowledge the financial support of "Fundação para a Ciência e a Tecnologia" (FCT – Portugal), through project UIDB/04625/2020 (funding the research unit CERIS).

References

Abbasi M., Khezri M., Rasmussen K.J.R., Schafer B.W. (2018). "Elastic buckling analysis of cold-formed steel built-up sections with discrete fasteners using the compound strip method", *Thin-Walled Structures*, **124**(March), 58-71.

Bebiano R., Gonçalves R. Camotim D. (2015). "A cross-section analysis procedure to rationalise and automate the performance of GBT-based structural analyses", *Thin-Walled Structures*, **92**(July), 29-47.

Camotim D., Gonçalves R., Basaglia C. (2022). "Developments on the GBT-based stability analysis of thin-walled members and structural Systems", *Analysis and Design of Plated Structures – Volume 1: Stability* (2nd edition), N.E. Shanmugam, C.M. Wang (Eds.), Woodhead Publishing (Series in Civil and Structural Engineering), Elsevier, Amsterdam, 133-175.

Fratamico D.C., Schafer B.W. (2014). "Numerical studies on the composite action and buckling behavior of built-up cold-formed steel columns", *Proceedings of the 22nd International Specialty Conference on Cold-formed Steel Design and Construction* (CCFSS – November 5-6, St. Louis, Missouri), 213-228.

Fratamico D.C., Torabian S., Zhao X., Rasmussen K.J.R., Schafer B.W. (2018a). "Experiments on the global buckling and collapse of built-up cold-formed steel columns", *Journal of Construction Steel Research*, **144**(May) 65-80.

Fratamico D.C., Torabian S., Zhao X., Rasmussen K.J.R., Schafer B.W. (2018b). "Experimental studs on the composite action in sheathed and bare built-up cold-formed steel columns", *Thin-Walled Structures*, **127**(June), 290-305.

Georgieva I., Schueremans L., Vandewalle L., Pyl L. (2012). "Design of built-up cold-formed steel columns according to the direct strength method", *Procedia Engineering*, **40** (Steel Structures and Bridges 2012), 119-124.

Gonçalves R., Camotim D., Basaglia C., Martins A.D., Peres N. (2023). "Latest developments on the analysis of thin-walled structures using Generalised Beam Theory (GBT)", *Journal of Constructional Steel Research*, **204**(May), paper 107858.

Khezri M., Rasmussen K.J.R. (2023). "Buckling mode decomposition of built-up members by the modal finite strip method (mFSM)", *Website Proceedings of the Structural Stability Research Council 2023 Annual Stability Conference* (SSRC 2023 – April 11-14, Charlotte, North Carolina).

Li Q.-Y., Young B. (2022). "Experimental and numerical investigation on cold-formed steel built-up section pin-ended columns", *Thin-Walled Structures*, **170**(January), paper 108444.

Li Q.-Y., Young B. (2023). "Numerical investigation and design of cold-formed steel built-up section beam-column members under moment gradients", *Engineering Structures*, **283**(May), paper 115746.

Li S., Schafer B. W. (2010). "Application of the finite strip method in cold-formed steel member design", *Journal of Constructional Steel Research*, **66**(8-9), 971-980.

Mahar A.M., Jayachandran S. A. (2021). "A computational study on buckling behavior of cold-formed steel built-up columns using compound spline finite strip method", *International Journal of Structural Stability and Dynamics*, **21**(5), paper 2150064.

Puckett J.A., Gutkowski R.M. (1986). “Compound strip method for analysis of plate systems”, *Journal of Structural Engineering* (ASCE), **112**(1), 121-138.

Rasmussen K.J.R., Krezri M., Schafer B.W., Zhang H. (2020). “The mechanics of built-up cold-formed steel members”, *Thin-Walled Structures*, **154**(September), paper 106756.

Selvaraj S., Madhavan M. (2022). “Experimental investigation and design considerations on cold-formed steel built-up I-section columns subjected to interactive buckling modes”. *Thin-Walled Structures*, **175**(June), paper 109262.

Stone T.A., LaBoube R.A. (2005). “Behavior of cold-formed steel built-up I-sections”, *Thin-Walled Structures*, **46**(12), 1805-1817.

Swanson Analysis Systems Inc. (2013). *ANSYS Reference Manual* (version 15).

Vy S.T., Mahendran M., Sivaprakasam T. (2021). “Built-up back-to-back cold-formed steel compression members failing by local and distortional buckling”. *Thin-Walled Structures*, **159**(February), paper 107224.

Yu W.-W., Laboube R.A., Chen H. (2019). *Cold-Formed Steel Design* (5th. Edition), Wiley, Hoboken.